

# Heterogeneous reaction of HO<sub>2</sub> with airborne TiO<sub>2</sub> particles and its implication for climate change mitigation strategies

Daniel R. Moon<sup>1</sup>, Giorgio S. Taverna<sup>2</sup>, Clara Anduix-Canto<sup>1</sup>, Trevor Ingham<sup>1,3</sup>, Martyn P. Chipperfield<sup>2,3</sup>, Paul W. Seakins<sup>1,3</sup>, Maria-Teresa Baeza-Romero<sup>4</sup>, Dwayne E. Heard<sup>1,3</sup>\*

<sup>1</sup> School of Chemistry, University of Leeds, Leeds, LS2 9JT, UK

<sup>2</sup> School of Earth and Environment, University of Leeds, LS2 9JT, UK

<sup>3</sup> National Centre for Atmospheric Science, School of Chemistry, University of Leeds, Leeds, LS2 9JT, UK

<sup>4</sup> Escuela de Ingeniería Industrial, Universidad de Castilla-La Mancha, 45071, Toledo, Spain

\* Corresponding author. Email: [d.e.heard@leeds.ac.uk](mailto:d.e.heard@leeds.ac.uk)

## Abstract.

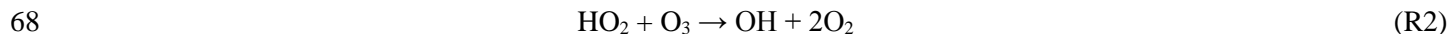
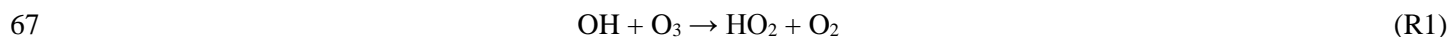
One geoengineering mitigation strategy for global temperature rises resulting from the increased concentrations of greenhouse gases is to inject particles into the stratosphere to scatter solar radiation back to space, with TiO<sub>2</sub> particles emerging as a possible candidate. Uptake coefficients of HO<sub>2</sub>,  $\gamma(\text{HO}_2)$ , onto sub-micrometre TiO<sub>2</sub> particles were measured at room temperature and different relative humidities (RH) using an atmospheric pressure aerosol flow tube coupled to a sensitive HO<sub>2</sub> detector. Values of  $\gamma(\text{HO}_2)$  increased from  $0.021 \pm 0.001$  to  $0.036 \pm 0.007$  as the RH was increased from 11% to 66%, and the increase in  $\gamma(\text{HO}_2)$  correlated with the number of monolayers of water surrounding the TiO<sub>2</sub> particles. The impact of the uptake of HO<sub>2</sub> onto TiO<sub>2</sub> particles on stratospheric concentrations of HO<sub>2</sub> and O<sub>3</sub> was simulated using the TOMCAT three-dimensional chemical transport model. The model showed that by injecting the amount of TiO<sub>2</sub> required to achieve the same cooling effect as the Mt. Pinatubo eruption, heterogeneous reactions between HO<sub>2</sub> and TiO<sub>2</sub> would have a negligible effect on stratospheric concentrations of HO<sub>2</sub> and O<sub>3</sub>.

## 27 **1. Introduction**

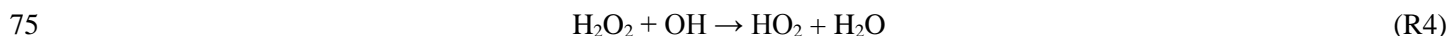
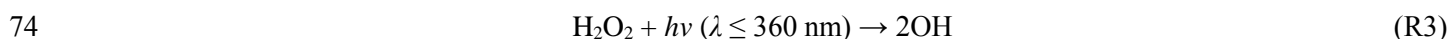
28 It has been suggested that injection of aerosols into the stratosphere in order to scatter solar radiation back to space  
29 could be a possible solar radiation management scheme (Shepherd and Working Group on Geoengineering the  
30 Climate, 2009). Such a scheme would have the effect of cooling the Earth's surface and serve as a measure to  
31 mitigate enhanced global warming. A possible candidate for stratospheric injection is sulphuric acid aerosols as these  
32 aerosols occur naturally in the stratosphere. These aerosols are formed by transport of precursors, e.g. SO<sub>2</sub> and  
33 carbonyl sulphide (OCS), from the troposphere to the stratosphere (Holloway and Wayne, 2010), which form  
34 sulphuric acid vapour that condenses onto particles. However, injection of these particles could have important  
35 negative effects on the stratosphere through enhanced ozone depletion. Concentrations of sulphate aerosols can  
36 increase dramatically as the result of volcanic eruptions. Following the eruption of Mt. Pinatubo in 1991, it was  
37 estimated that around 30 Tg of H<sub>2</sub>SO<sub>4</sub> was injected in the stratosphere, dramatically increasing stratospheric aerosol  
38 loading and hence the available surface area for heterogeneous chemistry to occur. Following this volcanic event,  
39 the average global lower tropospheric temperature decreased by 0.5 K (Dutton and Christy, 1992), however,  
40 stratospheric ozone concentrations reached a record low in northern mid-latitudes (Dutton and Christy,  
41 1992;McCormick et al., 1995) showing that sulphate aerosols could be unsuitable for solar radiation management.  
42 The impact of sulphate geoengineering to stratospheric ozone concentrations is projected to decrease in time as  
43 concentrations of Br and Cl containing atmospheric species are expected fall, so much so that beyond 2050 the  
44 additional available surface area provided by sulphate geoengineering is predicted to enhance conversion of NO<sub>x</sub>  
45 (NO<sub>x</sub> = NO + NO<sub>2</sub>) to HNO<sub>3</sub> resulting in an increase of stratospheric ozone (Visoni et al., 2017). Other candidates  
46 for particle types, such as TiO<sub>2</sub>, have been put forward due to their large refractive indices (Pope et al., 2012), meaning  
47 that less stratospheric aerosol loading would be necessary to achieve the same level of cooling. The refractive index  
48 of TiO<sub>2</sub> at 550 nm is 2.5 compared to a value of 1.5 for naturally occurring sulphate aerosols (Tang et al., 2014).  
49 Assuming that the size of TiO<sub>2</sub> particles can be optimised, it has been reported that to achieve the same cooling effect  
50 that sulphate aerosols had during the Mt. Pinatubo event, approximately three times less in mass, and seven times  
51 less in volume of TiO<sub>2</sub> would be required compared with sulphuric acid (Pope et al., 2012). However, the impacts  
52 of the presence of TiO<sub>2</sub> particles on stratospheric chemistry have to be determined before this kind of geoengineering  
53 solution can be considered. Mineral dust particles are commonly found in the troposphere and contribute the largest  
54 fraction to tropospheric aerosol loading in terms of mass (Textor et al., 2006;Huneus et al., 2011). Typically TiO<sub>2</sub>  
55 (which is classified as a mineral) constitutes from 0.1% to 10% of overall atmospheric mineral dust loading depending  
56 on the location of sources (Usher et al., 2003;Karagulian et al., 2006).

57 The heterogeneous chemistry of sulphate aerosols in the stratosphere is fairly well understood (Ammann et al., 2013);  
58 for example the conversion of NO<sub>x</sub> to nitric acid in the aerosol via N<sub>2</sub>O<sub>5</sub> adsorption and reaction, and also the  
59 activation of chlorine via the reaction of ClONO<sub>2</sub> with HCl to form Cl<sub>2</sub> and nitric acid within cold aerosols. However,  
60 the heterogeneous reactivity of mineral particles, in particular TiO<sub>2</sub>, is not as well understood. Removal and  
61 production of trace gases in the stratosphere may significantly perturb concentrations of O<sub>3</sub>, therefore it is important  
62 when assessing the potential impact of such a solar radiation management scheme to evaluate the kinetics of likely  
63 heterogeneous chemistry.

64 The hydroperoxyl radical, HO<sub>2</sub>, is an important species within the stratosphere, being present at about 5 parts per  
65 trillion per unit volume (pptv) around the tropopause, and is involved in a HO<sub>x</sub> catalytic cycle responsible for about  
66 40% of O<sub>3</sub> depletion in the lower stratosphere via to the following reactions (Wennberg, 1994):



70 Moreover, HO<sub>2</sub> can also react with stratospheric ClO and BrO to produce HOCl and HOBr respectively, which can  
71 be photolysed to produce further OH and atomic halogen species that can contribute to O<sub>3</sub> loss. HO<sub>2</sub> can undergo  
72 self-reaction upon surfaces of mineral dust, which is thought to result in the generation of H<sub>2</sub>O<sub>2</sub> (Matthews et al.,  
73 2014), whose two predominant removal pathways are photolysis and reaction with OH (Versick et al., 2012):



76 Although the kinetics of the uptake of HO<sub>2</sub> onto Arizona Test Dust (ATD), a proxy of mineral dust, has been  
77 previously investigated (Matthews et al., 2014;Bedjanian et al., 2013) the heterogeneous reaction of HO<sub>2</sub> with TiO<sub>2</sub>  
78 has not been studied. However, the kinetics of N<sub>2</sub>O<sub>5</sub> uptake (Tang et al., 2014) and ClONO<sub>2</sub> (Tang et al., 2016) onto  
79 TiO<sub>2</sub> have been studied. The heterogeneous reaction of N<sub>2</sub>O<sub>5</sub> results in the conversion to reactive nitrogen oxides  
80 (NO and NO<sub>2</sub>) involved in a catalytic cycle that leads to significant O<sub>3</sub> depletion and non-reactive HNO<sub>3</sub>. The reactive  
81 uptake coefficient,  $\gamma$ , which is the probability that a species will collide with an aerosol and be removed by reaction,  
82 was measured to be more than an order of magnitude larger for HO<sub>2</sub> onto ATD than for N<sub>2</sub>O<sub>5</sub> and ClONO<sub>2</sub> onto TiO<sub>2</sub>  
83 sub-micron particles, and contrasting dependences of  $\gamma$  with relative humidities (RH) were observed. Therefore, by  
84 analogy it is expected that HO<sub>2</sub> uptake onto TiO<sub>2</sub> may be faster than N<sub>2</sub>O<sub>5</sub> uptake. ClONO<sub>2</sub> uptake by TiO<sub>2</sub> particles  
85 resulted in similar values of  $\gamma$ , however, no dependency of  $\gamma$  with RH between 7 – 33% was observed.

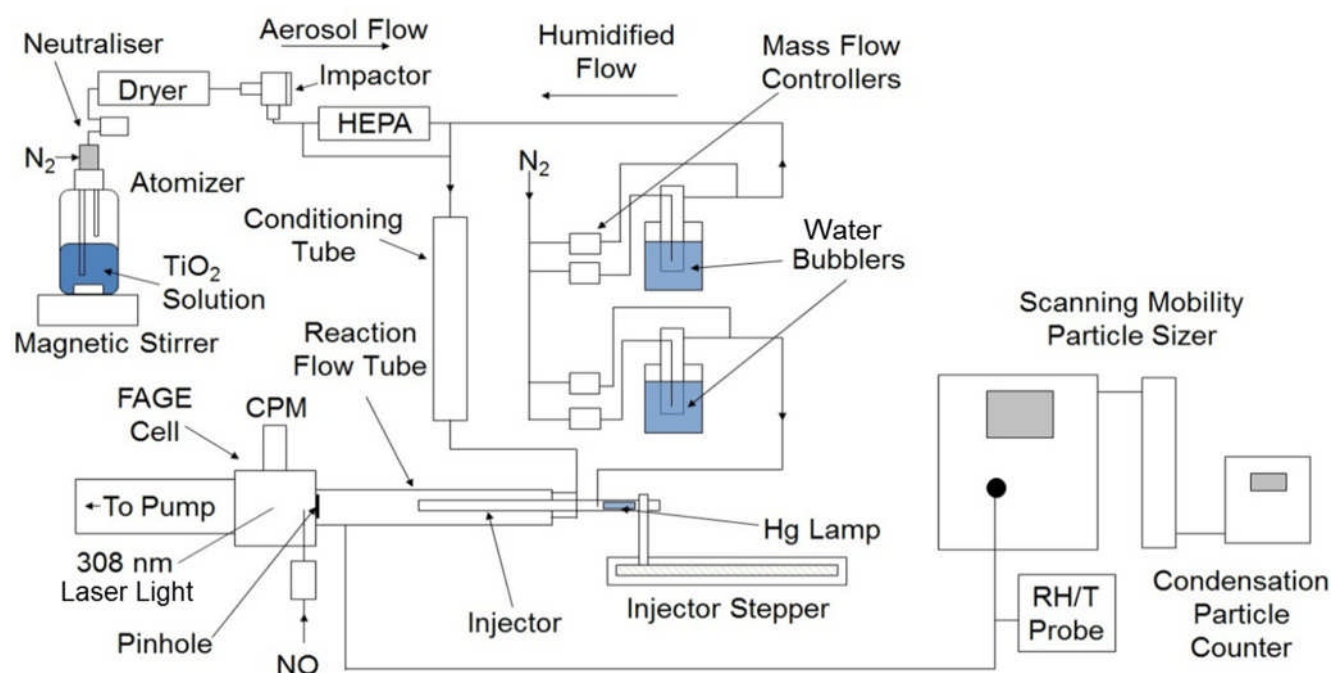
86 In this investigation a borosilicate glass aerosol flow tube coupled with a sensitive HO<sub>2</sub> detector based on chemical  
87 conversion followed by laser-induced fluorescence detection of OH (George et al., 2013) has been used to study the  
88 kinetics of the heterogeneous reaction of HO<sub>2</sub> with airborne TiO<sub>2</sub> nanoparticles at different RH. While it has been  
89 possible here to study such kinetics over a range of RH representative to those typically found in the lower  
90 stratosphere (< 40%) (Wennberg, 1994), experimental limitations meant that experiments were only conducted at  
91 room temperature (~293 K). The TOMCAT off-line three-dimensional (3D) chemical transport model (Chipperfield;  
92 1999) has also been used to predict the likely impact of HO<sub>2</sub> uptake by TiO<sub>2</sub> particles on the stratospheric  
93 concentrations of HO<sub>2</sub> and O<sub>3</sub>.

94

95 **2. Methods.**

96 **2.1. Overview of experimental apparatus**

97 The experimental setup deployed for this investigation is similar to other investigations of HO<sub>2</sub> uptake by aerosols  
98 undertaken at the University of Leeds (George et al., 2013; Matthews et al., 2014; Lakey et al., 2016) therefore a  
99 detailed description of the components of the experiment is not given. A schematic diagram of the experiment is  
100 shown in Figure 1, and all experiments were undertaken at room temperature (293 ± 3 K) and under normal laboratory  
101 levels of illumination. For some experiments the flow tube was covered with a black shield to eliminate light and no  
102 differences in the results were observed.



103  
104 **Figure 1.** Schematic diagram of the aerosol flow tube experiment. CPM: Channel Photomultiplier, HEPA: high-  
105 efficiency particulate air filter, FAGE: fluorescence assay by gas expansion, RH/T: Relative Humidity/Temperature.

106  
107 Compressed nitrogen, which had been passed through a gas purification system (TSI 3074B) consisting of particle  
108 filters, a dryer and a carbon filter, was used as the carrier gas for the experiments. A humidified flow of TiO<sub>2</sub> particles  
109 was introduced through two inlets located at the rear of the aerosol flow tube and the flow of HO<sub>2</sub> radicals enters the  
110 flow tube via the movable injector. The total flow through the flow tube (107 cm length, 5.9 cm I.D.) was 5.4 L  
111 min<sup>-1</sup> which resulted in a Reynolds number of 130, and therefore is considered laminar as confirmed by radial  
112 concentration gradient measurements of gases exiting the injector (George et al., 2013). Experiments consisted of  
113 moving the injector using a linear drive (BSL Engineering 15 KR4610A) to different fixed positions along the flow  
114 tube (30-70 cm from injector tip to HO<sub>2</sub> detector inlet in steps of 5 cm) corresponding to reaction times between ~ 8  
115 and 20 s from the injector, with detection of HO<sub>2</sub> at the end of the flow tube. All gas flows within the experiment  
116 were controlled using mass flow controllers (Brookes and MKS). The RH of the flow was measured using a probe

117 (Rotronics) in the exhaust of the flow tube, which itself was calibrated against a dew point hygrometer (Buck  
118 Research Instruments CR-4).

119

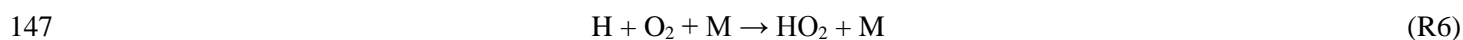
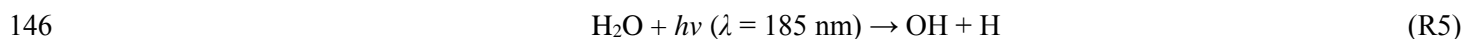
## 120 **2.2. Aerosol Generation and Detection**

121 A solution of TiO<sub>2</sub> (Aldrich Chemistry 718467, 99.5% Degussa i.e. a blend of TiO<sub>2</sub> polymorphs 80% anastase and  
122 20% rutile, 5 g in 500 ml of Milli-Q water) was placed in a commercial atomizer (TSI 3076) in order to produce a 1  
123 L min<sup>-1</sup> flow entrained with TiO<sub>2</sub> particles, referred to as the aerosol flow. The aerosol flow was then passed through  
124 a neutraliser (Grimm 5522) to reduce static wall losses, a diffusion drier (TSI 3062) and an impactor (TSI 1035900)  
125 to ensure larger aerosols, beyond the detection range of the SMPS (~ 750 nm diameter), do not enter the aerosol flow  
126 tube. A high-efficiency particulate air (HEPA, PALL Life Sciences) filter situated within a by-pass loop was used  
127 to control the number concentration of particles entering the aerosol flow tube. The aerosol flow was then mixed  
128 with a humidified flow of nitrogen (3 L min<sup>-1</sup>) to control the RH within the system. The RH of the humidified flow  
129 was altered by changing the ratio of dry nitrogen and nitrogen passed through a water bubbler. This flow was then  
130 passed through a conditioning tube (residence time ~ 6 s) before entering the aerosol flow tube to allow time for  
131 water adsorption onto the surface of the TiO<sub>2</sub> particles to equilibrate at the given RH.

132 The total surface area of TiO<sub>2</sub> particles available for heterogeneous reaction with HO<sub>2</sub> was measured with a SMPS  
133 instrument from the flow exiting the aerosol flow tube. Previous experiments showed that there is a negligible loss  
134 of aerosols during the transit of the flow tube (George et al., 2013). The SMPS consisted of a Differential Mobility  
135 Analyzer (DMA, TSI 3080, 3081) that creates a monodisperse flow of aerosols based on their electrical mobility  
136 which is related to their size. A condensation particle counter (CPC, TSI 3775) connected in parallel to the DMA  
137 quantified particle number concentrations. These two instruments connected in parallel can be used to create an  
138 aerosol size distribution from which the total surface area and average radius of particles can be calculated by making  
139 the assumption that particles are spherical (as demonstrated experimentally in section 3.2 below). The average  
140 diameter of the particles is 136 nm and 173 nm at RH = 11% and 37%, respectively.

## 141 **2.3 HO<sub>2</sub> Generation and Detection**

142 HO<sub>2</sub> radicals were produced within the movable injector (110 cm length, 1.9 cm O.D., 1.6 cm I.D.) by passing a 1.3  
143 L min<sup>-1</sup> humidified flow of nitrogen (consisting of a mixture of 0.9 L min<sup>-1</sup> of dry N<sub>2</sub> and 0.4 L min<sup>-1</sup> N<sub>2</sub> passed  
144 through a water bubbler) containing trace amounts of oxygen over a mercury lamp (L.O.T.-Oriol 6035) via the  
145 following reactions:



148 OH is also created by the photolysis of water vapour in R5, but no OH was observed exiting the injector, presumably  
149 owing to rapid losses at the walls of the injector. HO<sub>2</sub> was sampled by a 0.7 mm diameter pinhole at the end of the  
150 flow tube, and after chemical conversion to OH by addition of excess NO (50 sccm, BOC, 99.5 %) just inside the

151 pinhole, laser induced fluorescence (LIF) at low-pressure (the fluorescence assay by gas expansion (FAGE) technique  
152 (Heard and Pilling, 2003)) was used to measure OH. The relative LIF signal from converted HO<sub>2</sub> was calibrated  
153 using an established method (Winiberg et al., 2015) developed for field measurements of OH and HO<sub>2</sub> radicals.  
154 Hence the experiment is able to measure the absolute concentration of HO<sub>2</sub> during passage from the injector to the  
155 sampling inlet. The Q<sub>1</sub>(2) line of the OH ( $A^2\Sigma^+ v' = 0 - X^2\Pi_{1-} v'' = 0$ ) transition at ~ 308 nm was used to detect OH.  
156 A Nd:YAG pumped dye laser (JDSU Q201-HD Q-series, Sirah Cobra Stretch) was used to produce the required 308  
157 nm radiation (line width ~ 0.1 cm<sup>-1</sup>) at a pulse repetition rate of 5 kHz. As the flows through the movable injector  
158 (1.3 L min<sup>-1</sup>) and mercury lamp current (20 mA) were kept constant, it is assumed that the initial HO<sub>2</sub> concentration,  
159 [HO<sub>2</sub>]<sub>0</sub> (defined in this investigation as [HO<sub>2</sub>] at the first injector position, i.e. 30 cm downstream of the injector),  
160 determined by calibration to be 1.6 × 10<sup>9</sup> molecule cm<sup>-3</sup>, was the same for all experiments. These HO<sub>2</sub> concentrations  
161 are ~ 50 times higher than typical levels in the sunlit stratosphere (Wennberg et al., 1994). A reference fluorescence  
162 cell, in which a large concentration of OH was generated and detected by LIF, was used to facilitate the identification  
163 of OH lines and tune the laser wavelength. The FAGE cell was continuously evacuated using a combination of a  
164 rotary pump (Edwards, model E1M80) and a roots blower (EH1200), and was kept at 0.8–0.9 Torr, which was  
165 monitored using a capacitance monitor (Tylan General, CDC 11).

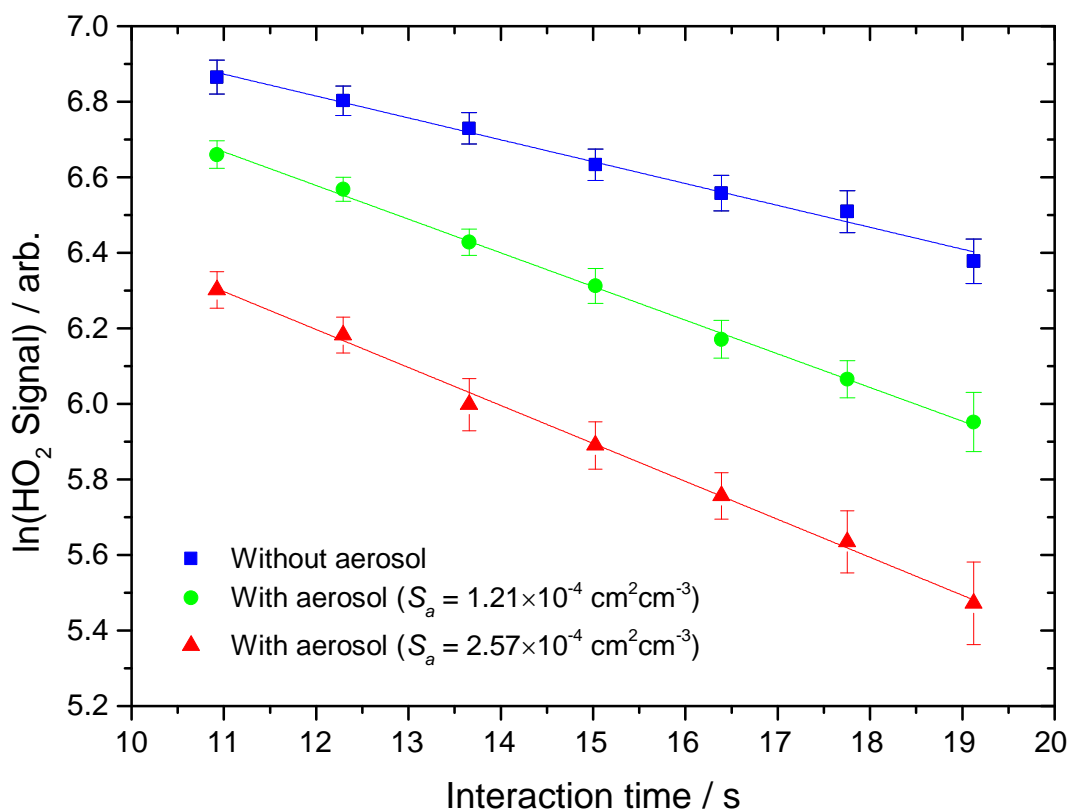
## 166 2.4. Experimental Procedure and Data Analysis

167 The HO<sub>2</sub> signal was measured at 8 positions as the moveable injector was drawn back from 30 to 70 cm using the  
168 linear stepper drive and again as the moveable injector was pushed forwards back to its initial position. The HO<sub>2</sub>  
169 signal was averaged over 20 s (average of twenty 1 s measurement points, each corresponding to 5000 laser shots) at  
170 each injector position with a 22 s delay between measurements at each injector position in order to allow time for  
171 mechanical vibrations to subside, and to ensure a full flush of the aerosol flow tube so that the LIF signal corresponds  
172 to HO<sub>2</sub> emitted from the injector position being measured. The laser power was recorded for each injector position  
173 and used to normalise the HO<sub>2</sub> signal to correct for any fluctuations in laser power (< 5%). The HO<sub>2</sub> signals with the  
174 injector moving forwards and backwards were then averaged, and this procedure repeated six times with varying  
175 concentrations of aerosols present in the aerosol flow tube. The wall loss rate of HO<sub>2</sub> ( $k_{\text{wall}}$ ) was determined by  
176 recording the HO<sub>2</sub> decay in the absence of aerosols, but at the same RH, and was repeated four times for each  
177 experiment.

178 The HO<sub>2</sub> concentration as a function of time along the flow tube can be expressed as:

$$179 \quad \ln[\text{HO}_2]_t = \ln[\text{HO}_2]_0 - k_{\text{obs}} t \quad (\text{Eqn. 1})$$

180 where [HO<sub>2</sub>]<sub>t</sub> and [HO<sub>2</sub>]<sub>0</sub> are concentrations of HO<sub>2</sub> at time  $t$  and  $t = 0$  respectively, and  $k_{\text{obs}}$  is the observed pseudo-  
181 first-order rate coefficient for HO<sub>2</sub> uptake. As the HO<sub>2</sub> signal is directly proportional to the concentration of HO<sub>2</sub>,  
182 the gradient of a plot of ln(HO<sub>2</sub> Signal) against time (calculated from the injector position and measured flow rate)  
183 yields  $k_{\text{obs}}$ , as shown in Figure 2.



184

185 **Figure 2.** Measured HO<sub>2</sub> signal at different interaction times, in the presence of TiO<sub>2</sub> particles (surface area density  
 186  $1.21 \times 10^{-4} \text{ cm}^2 \text{ cm}^{-3}$  and  $2.57 \times 10^{-4} \text{ cm}^2 \text{ cm}^{-3}$ , green circles and red triangles respectively) and in their absence (blue  
 187 squares). The RH in the aerosol flow tube was 11%, the lowest used in this study. The lines represent linear-least  
 188 squares fits to the data yielding  $k_{\text{obs}} = 0.079 \pm 0.005 \text{ s}^{-1}$  and  $k_{\text{obs}} = 0.093 \pm 0.003 \text{ s}^{-1}$  (aerosols present, green circles  
 189 and red triangles respectively) and  $0.049 \pm 0.003 \text{ s}^{-1}$  (no aerosols,  $k_{\text{wall}}$ ).

190 The flow tube was coated with halocarbon wax (Halocarbon Products Corporation, Halocarbon Wax Series 600) to  
 191 reduce HO<sub>2</sub> wall loss rate ( $k_{\text{wall}}$ ) and an average of  $k_{\text{wall}}$  from several determinations in the absence of aerosols was  
 192 subtracted from  $k_{\text{obs}}$ . A correction (typically about 30%) to account for non-plug flow conditions in the aerosol flow  
 193 tube using the procedure outlined by Brown (Brown, 1978) was applied to yield,  $k'$ , the pseudo-first-order loss of  
 194 HO<sub>2</sub> by heterogeneous reaction with TiO<sub>2</sub> particles. The relationship between  $k'$  and total surface area of TiO<sub>2</sub>  
 195 particles ( $S_a$ ) can be expressed as (George et al., 2013):

$$196 \quad k' = \frac{w_{\text{HO}_2} \gamma_{\text{obs}} S_a}{4} \quad (\text{Eqn. 2})$$

197 where  $w_{\text{HO}_2}$  is the mean velocity of HO<sub>2</sub> ( $\sim 435 \text{ ms}^{-1}$  at 293 K) and  $\gamma_{\text{obs}}$  is the observed reactive uptake coefficient,  
 198 obtained from a plot of  $k'$  versus  $S_a$ , an example of which is given in Figure 3.  $\gamma_{\text{obs}}$  was in turn corrected (typically  
 199  $\sim 1\%$ ) to account for the gas diffusion limitation (Fuchs and Sutugin, 1970), to yield  $\gamma(\text{HO}_2)$ .

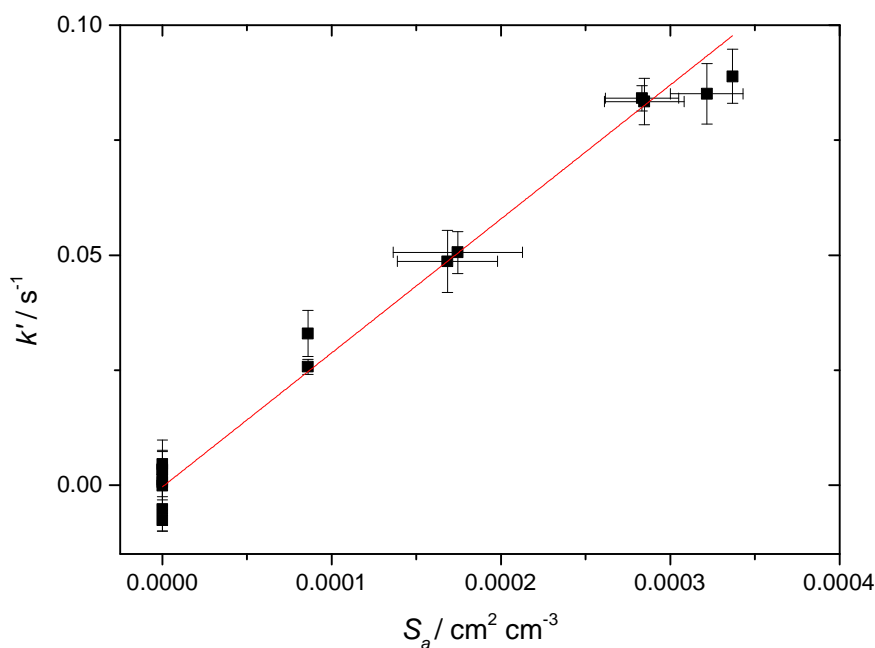


**Figure 3.** First order rate coefficient for loss of HO<sub>2</sub> due to heterogeneous reaction with TiO<sub>2</sub> particles at different total surface areas for T = 296 K and RH = 37%. The gradient yielded a value of  $\gamma(\text{HO}_2) = (2.68 \pm 0.01) \times 10^{-2}$ , with the uncertainty representing 2 $\sigma$  random errors from the fit (95% confidence limits).

## 2.5. TOMCAT Model Description

The TOMCAT off-line three-dimensional (3D) chemical transport model (CTM) (Chipperfield, 1999, 2006) has been used to predict the impact of the heterogeneous reaction of TiO<sub>2</sub> with HO<sub>2</sub> to stratospheric concentrations of O<sub>3</sub> and HO<sub>2</sub>. The model has been widely used in previous studies of stratospheric chemistry and performs well in reproducing stratospheric ozone and the trace species which control its distribution (Chipperfield et al., 2015). The model includes a detailed treatment of stratospheric chemistry of O<sub>x</sub>, HO<sub>x</sub>, NO<sub>y</sub>, Cl<sub>y</sub> and Br<sub>y</sub> species along with the main source gases. The model has a comprehensive gas-phase chemistry scheme and includes a number of heterogeneous reactions on stratospheric sulphate aerosols and polar stratospheric clouds (Chipperfield, 1999).

The loss rate of HO<sub>2</sub> due to heterogeneous reaction with TiO<sub>2</sub> was included in the model as:

$$k = 0.25 S_a w_{\text{HO}_2} \gamma(\text{HO}_2) \quad (\text{Eqn. 3})$$

where  $S_a$  is the surface area density of TiO<sub>2</sub>, and  $w_{\text{HO}_2}$  and  $\gamma(\text{HO}_2)$  are defined above. Three TOMCAT simulations were performed at a horizontal resolution of  $5.6^\circ \times 5.6^\circ$  and 32 levels from the surface to ~ 60 km. The model was forced with wind and temperature fields from the European Centre for Medium-Range Weather Forecasts (ECMWF) ERA-Interim reanalyses and integrated for 2 years from January 2007 until December 2008, initialised with the output from a standard TOMCAT run which had spun-up from 1977. More information on the model experiments is given in Section 3.3.



222 **3. Results and Discussion**

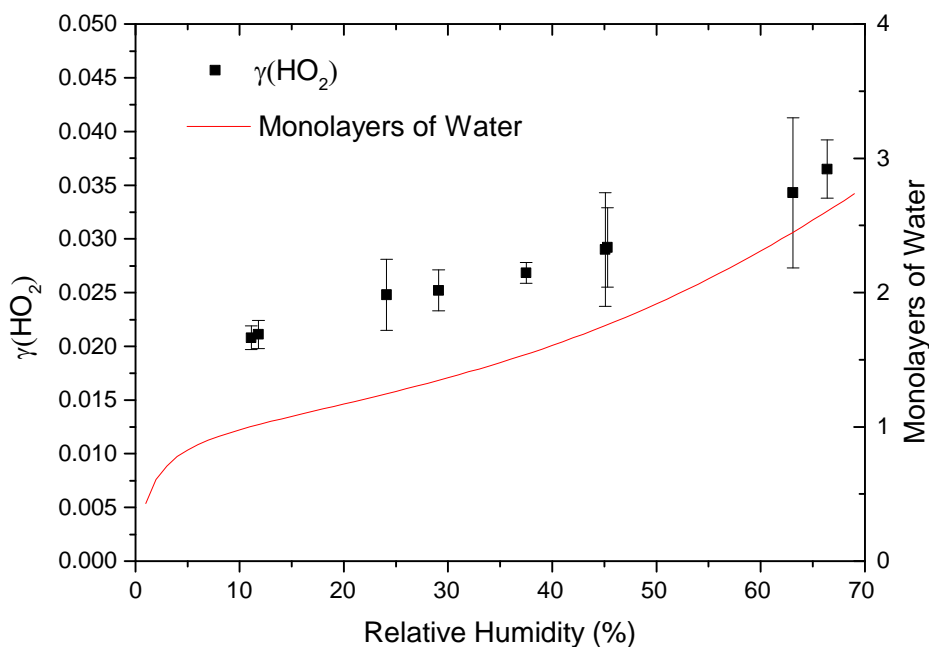
223 **3.1. The reactive uptake coefficient dependence with relative humidity**

224 The reactive uptake coefficient for HO<sub>2</sub> radicals,  $\gamma(\text{HO}_2)$ , onto TiO<sub>2</sub> particles was determined at eight different RH  
 225 (11 - 66%), as shown in Figure 4 and summarised in Table 1. The number of monolayers of water adsorbed onto the  
 226 surface of TiO<sub>2</sub> particles has been previously determined experimentally by transmission FTIR spectroscopy  
 227 (Goodman et al., 2001), and is also shown as a function of RH in Figure 4.

228 **Table 1.** Reactive HO<sub>2</sub> uptake coefficients,  $\gamma(\text{HO}_2)$ , for TiO<sub>2</sub> particles at different RH.

RH (%) $\pm$ 1.0	$\gamma(\text{HO}_2) \times 10^{-2}$
11.1	2.08 $\pm$ 0.11
11.8	2.11 $\pm$ 0.13
24.9	2.48 $\pm$ 0.33
29.1	2.54 $\pm$ 0.18
37.5	2.68 $\pm$ 0.09
45.1	2.90 $\pm$ 0.53
45.3	2.92 $\pm$ 0.37
63.1	3.43 $\pm$ 0.27
66.4	3.65 $\pm$ 0.70

229



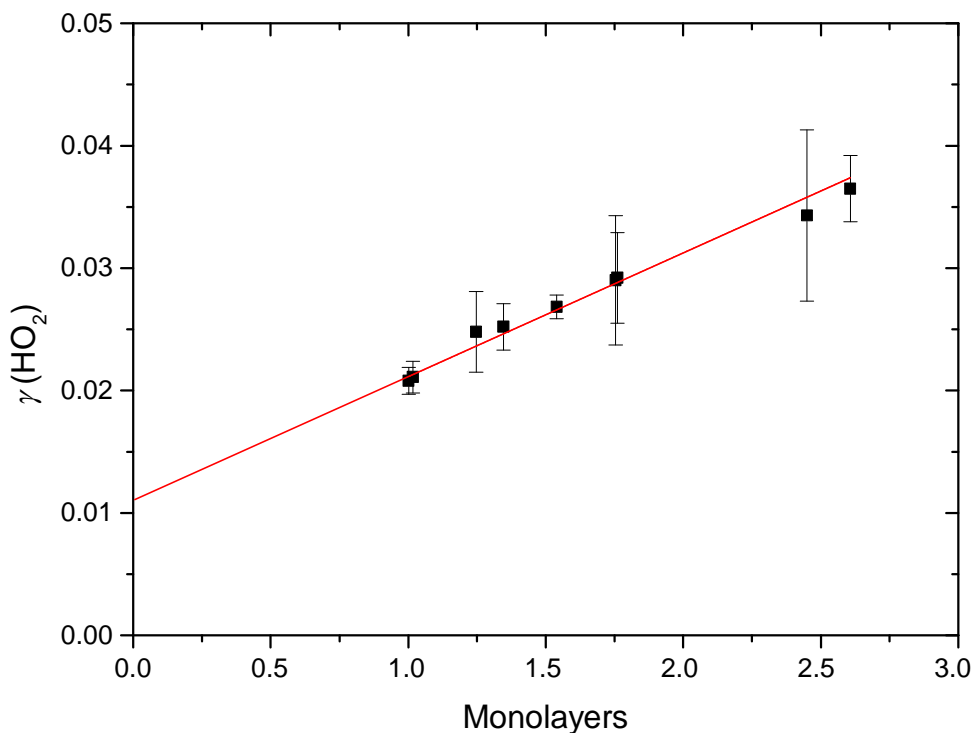
230

231 **Figure 4.** Reactive uptake coefficients of HO<sub>2</sub>,  $\gamma(\text{HO}_2)$ , onto airborne TiO<sub>2</sub> particles (black squares, left y axis) at  
 232 different RH for  $T = 295 \pm 2$  K. The number of monolayers of the adsorbed water on TiO<sub>2</sub> particles (red curve, right  
 233 y axis) at 296 K is also plotted as a function of RH, determined using FTIR spectroscopy (Goodman et al., 2001).

234 The results clearly show a positive dependence of  $\gamma(\text{HO}_2)$  across the range of RH investigated, and as shown in Figure  
 235 5,  $\gamma(\text{HO}_2)$  correlates well with the number of monolayers of water adsorbed onto the  $\text{TiO}_2$  particles,  $V/V_m$ , determined  
 236 by Goodman *et al.* (2001), and which was parameterised by Eqn. 4:

$$237 \quad \frac{V}{V_m} = \left[ \frac{c\left(\frac{P}{P_0}\right)}{1-\left(\frac{P}{P_0}\right)} \right] \left[ \frac{1-(n+1)\left(\frac{P}{P_0}\right)^n + n\left(\frac{P}{P_0}\right)^{n+1}}{1+(c-1)\left(\frac{P}{P_0}\right) - c\left(\frac{P}{P_0}\right)^{n+1}} \right] \quad (\text{Eqn. 4})$$

238 where  $V$  is the volume of gas (water vapour) adsorbed at equilibrium pressure  $P$ ,  $V_m$  is volume of gas necessary to  
 239 cover the surface of the adsorbent  $\text{TiO}_2$  particles with a complete monolayer,  $P$  is the equilibrium pressure of the  
 240 adsorbing gas,  $P_0$  is the saturation vapour pressure of the adsorbing gas at that temperature,  $c$  is a temperature-  
 241 dependent constant related to the enthalpies of adsorption of the first and higher layers and  $n$  is the asymptotic limit  
 242 of monolayers ( $\sim 8$ ).



243

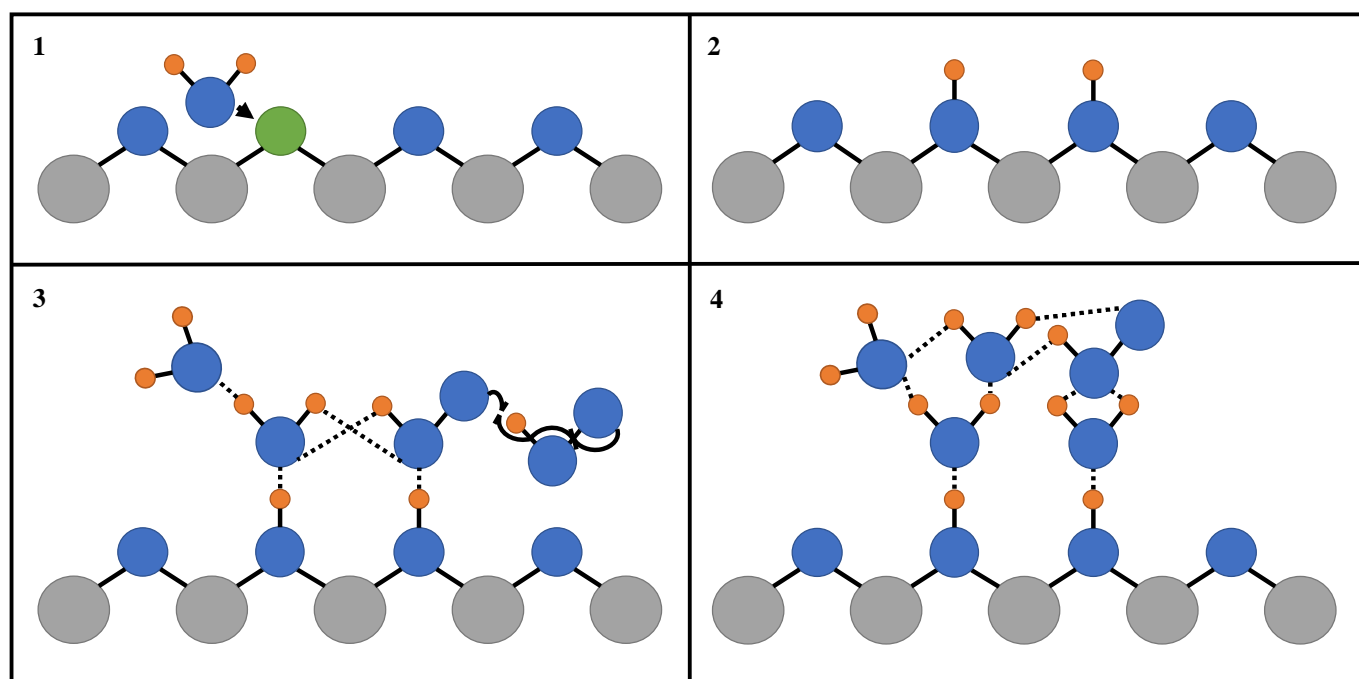
244 **Figure 5.** Variation of the reactive uptake coefficient,  $\gamma(\text{HO}_2)$ , with the number of monolayers of water surrounding  
 245  $\text{TiO}_2$  particles (as determined by Goodman *et al.*, 2001) for  $T = 295 \pm 2$  K. The red line represents a linear least-  
 246 squares fit to the data ( $r^2 = 0.987$ ).

247

248 Wall losses of  $\text{HO}_2$  also increase as RH is increased within the aerosol flow tube, and so in the absence of aerosols,  
 249 the  $[\text{HO}_2]$  for a given distance from the injector will decrease with RH. Previous work in this laboratory has shown  
 250 that  $\gamma(\text{HO}_2)$  for uptake on ATD aerosols increases as the  $[\text{HO}_2]$  is lowered (Matthews *et al.*, 2014), and hence some  
 251 of the positive dependence of  $\gamma(\text{HO}_2)$  with RH shown in Figure 4 might be expected simply owing to the  $[\text{HO}_2]$   
 252 impinging on the aerosol for a given injector position decreasing with RH. To investigate this further, uptake onto

253  $\text{TiO}_2$  at  $\text{RH} = 11\%$  was measured as a function of  $[\text{HO}_2]_0$  exiting the injector, and  $\gamma(\text{HO}_2)$  increased from  $2.08 \times 10^{-2}$   
 254 to  $2.72 \times 10^{-2}$  as  $[\text{HO}_2]_0$  was decreased from  $1.6 \times 10^9$  molecule  $\text{cm}^{-3}$  to  $8.9 \times 10^8$  molecule  $\text{cm}^{-3}$ . However, the wall  
 255 loss rate for  $\text{HO}_2$  only increased from  $0.049$  to  $0.079$   $\text{s}^{-1}$  across the entire range of  $\text{RH}$  (11% to 66%) resulting in only  
 256 a small change in  $[\text{HO}_2]$ , decreases of  $\sim 2.6 \times 10^8$  molecule  $\text{cm}^{-3}$  and  $\sim 2.7 \times 10^8$  molecule  $\text{cm}^{-3}$  at the first and last  
 257 injector position, respectively. In previous studies of  $\text{HO}_2$  uptake onto ATD (Matthews et al., 2014) it was shown  
 258 that the increase of  $\gamma(\text{HO}_2)$  with decreasing  $[\text{HO}_2]$  is linear. Therefore, assuming the same behaviour for uptake onto  
 259  $\text{TiO}_2$  particles, the expected change in  $\gamma(\text{HO}_2)$  as a result of  $\text{RH}$  increasing from 11-66% due only to a change in  
 260 initial  $\text{HO}_2$  concentration is only  $\Delta\gamma(\text{HO}_2)=0.0023$  (or  $\sim 6\%$  of the averaged measured  $\gamma(\text{HO}_2)$  across this range).  
 261 Hence the 75 % increase in  $\gamma(\text{HO}_2)$  observed in Figure 4 across this range of  $\text{RH}$  is due to another reason.

262 Figure 5 shows that, for the range of  $\text{RH}$  studied,  $\gamma(\text{HO}_2)$  is a linear function of the number of monolayers of water  
 263 surrounding a  $\text{TiO}_2$  particle, suggesting that water plays a role in the reactive  $\text{HO}_2$  uptake process on  $\text{TiO}_2$  particles.  
 264 Studies using ambient pressure photoelectron spectroscopy (APPEs) (Yamamoto et al., 2008) have shown that water  
 265 adsorption on rutile, a polymorph of  $\text{TiO}_2$  (110), occurs in distinct steps, as illustrated in Figure 6.



266

267 **Figure 6.** Simplified diagram of the important steps of  $\text{HO}_2$  reactive uptake onto the surface of  $\text{TiO}_2$ . Grey circles  
 268 = Ti, blue circles = O, orange circles = H, green circles = oxygen vacancy ( $V_{\text{bridge}}$ ), solid black lines = chemical  
 269 bond and dashed lines = hydrogen bond. Panel 1 shows the diffusion of water molecule towards a bridging O  
 270 vacancy. Panel 2 shows the resultant formation of two neighbouring bridging OH groups at the original site of the  
 271 O vacancy. Panel 3 shows the bridging OH groups acting as anchoring sites for water and  $\text{HO}_2$  adsorption via  
 272 hydrogen bonding leading to multilayer water adsorption and  $\text{HO}_2$  self-reaction via an Eley-Rideal type  
 273 mechanism. Panel 4 shows the build-up of a more extensive hydrogen bonded network as more water molecules  
 274 adsorb onto the particle, which stabilises  $\text{HO}_2$  increasing its desorption lifetime and hence probability that it will  
 275 react.

276 First, water molecules dissociate at O-vacancies ( $V_{\text{bridge}}$ ) in bridge sites, producing a stoichiometric amount of  
277 adjacent bridging OH groups ( $\text{OH}_{\text{bridge}}$ ) equal to twice the initial vacancy concentration upon initial exposure of rutile  
278 to water vapour:



280 This step takes place even at very low RH, with these bridging OH groups acting as nucleation sites for subsequent  
281 water adsorption by anchoring water molecules to form strongly bound  $\text{OH-H}_2\text{O}$  complexes. The  $\text{OH-H}_2\text{O}$   
282 complexes continue to act as nucleation centres for further water adsorption. The wetting properties of  $\text{TiO}_2$  (110)  
283 are thus driven by moderate amounts of strongly attractive OH sites that nucleate water molecules. These  $\text{OH-H}_2\text{O}$   
284 complexes have a relatively high enthalpy of adsorption for water of  $-72 \text{ kJ mol}^{-1}$  (Ketteler et al., 2007), whereas  
285 additional adsorption of water beyond a monolayer of water coverage is more characterised by enthalpies associated  
286 with the bulk enthalpy of water condensation ( $-45 \text{ kJ mol}^{-1}$ ) (Chen et al., 2012), explaining the variation of the number  
287 of monolayers of water with RH shown in Figure 4. Computational studies (Aloisio and Francisco, 1998) showed  
288 that in the gas-phase  $\text{HO}_2$  can also readily form complexes with water through hydrogen bonding with a binding  
289 energy of  $28.9 \text{ kJ mol}^{-1}$ . The observed correlation of  $\gamma(\text{HO}_2)$  with the number of monolayers of water surrounding  
290  $\text{TiO}_2$  particles could be explained by two effects. An increase in the network of hydrogen bonding would increase  
291 the stability of a molecular system,  $\sim 20.9 \text{ kJ mol}^{-1}$  for each hydrogen bond (Joshi and Ghanty, 2013), or that simply  
292 more  $\text{HO}_2$  can adsorb onto the particle surface as the number of available sites for hydrogen bonding increases. An  
293 increase in the adsorption lifetime of  $\text{HO}_2$  owing to the more extended H-bonding network (Joshi and Ghanty, 2013)  
294 will result in an increased probability of  $\text{HO}_2$  reacting with another  $\text{HO}_2$ , increasing the value of  $\gamma(\text{HO}_2)$ :



296 For up to  $\sim 2$  monolayers of  $\text{H}_2\text{O}$ , an Eley-Rideal (ER) mechanism of a gas phase  $\text{HO}_2$  molecule reacting an adsorbed  
297  $\text{HO}_2$  is more likely than for two adsorbed  $\text{HO}_2$  molecules diffusing together to react via a Langmuir-Hinshelwood  
298 (LH) mechanism. The coverage of  $V_{\text{bridge}}$  across the surface of  $\text{TiO}_2$  (110) is 0.125 monolayers (i.e. one vacancy for  
299 every eight unit cells) (Ketteler et al., 2007) meaning water will initially adsorb onto the surface of the particle in  
300 clusters. As the binding energy of the  $\text{HO}_2$  water complex is fairly high, the rate of  $\text{HO}_2$  diffusion across the surface  
301 after the initial adsorption at a bridging site will be slow, making a LH type mechanism seem unlikely. Above  $\sim 2$   
302 monolayers, the adsorbed water clusters will begin to interact with each other via an extended H-bonded network  
303 more characteristic of bulk liquid water, allowing  $\text{HO}_2$  to diffuse around the thin surface film of water with  
304 thermodynamic properties similar to liquid water (Ketteler et al., 2007).

305 The superoxide ion,  $\text{O}_2^-$ , which is the conjugate base of  $\text{HO}_2$ , reacts with  $\text{HO}_2$  over a hundred times quicker than with  
306  $\text{HO}_2$  via:



308 It is unlikely that  $\text{O}_2^-$  will form readily on the surface of the particle at low coverages of water.  $\text{O}_2^-$  can form on  
309 surfaces via direct surface-oxygen electron transfer, photo-induced electron transfer, surface intermolecular electron

310 transfer or decomposition of hydrogen peroxide ( $\text{H}_2\text{O}_2$ ) (Anpo et al., 1999). The dissociation of  $\text{HO}_2$  to  $\text{O}_2^-$  occurs in  
311 bulk liquid ( $pK_a = 4.7$ , (Thornton and Abbatt, 2005)), however, water surrounding the particles only begins to acquire  
312 liquid like properties once the coverage of water is greater than  $\sim 2$  monolayers. If significant formation of  $\text{O}_2^-$  does  
313 occur above  $\sim 2$  monolayers of  $\text{H}_2\text{O}$ , then owing to its much higher reactivity, some deviation from linearity of  $\gamma(\text{HO}_2)$   
314 versus monolayers of water (Figure 5) might be expected. However, this was not observed, although the number of  
315 data points is very limited.

316

### 317 **3.2. Comparison of $\gamma(\text{HO}_2)$ with literature values**

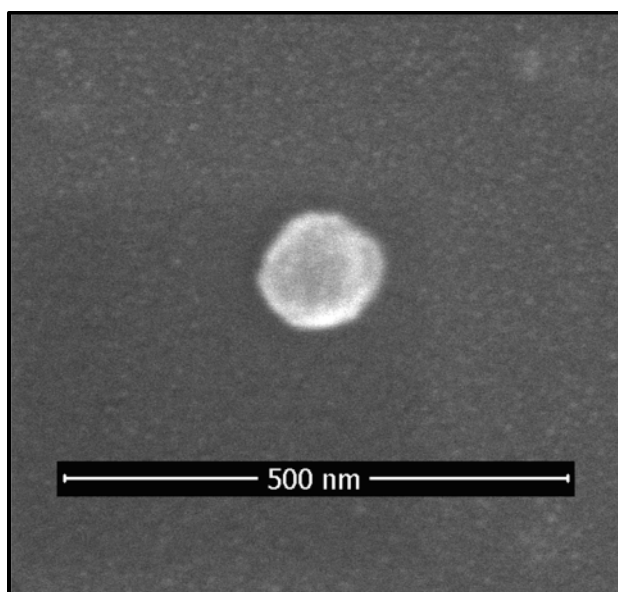
318 There are previous studies of  $\text{HO}_2$  uptake onto ATD (Matthews et al., 2014), a proxy for mineral dust, and both  $\text{N}_2\text{O}_5$   
319 (Tang et al., 2014) and  $\text{ClONO}_2$  (Tang et al., 2016) uptake onto  $\text{TiO}_2$  particles. Values of  $\gamma(\text{HO}_2)$  measured for ATD  
320 are comparable to those measured onto  $\text{TiO}_2$  particles at similar concentrations of  $\text{HO}_2$  in the aerosol flow tube  
321 ( $\gamma(\text{HO}_2)_{\text{ATD}} \sim 0.008 - 0.030$ ). For ATD,  $\gamma(\text{HO}_2)$  was only determined at 4 values of RH, but a general increase with  
322 RH was observed (although there was a dip around RH = 50% before a further increase), consistent with  $\text{HO}_2$  uptake  
323 being driven by the number of defects in the crystal lattice of mineral dust surfaces which provides bridging OH  
324 groups upon exposure to water and subsequently by the number of monolayers of water adsorbed onto the surface of  
325 such aerosols. The number of monolayers of water on the ATD surface at different RH has been determined  
326 (Gustafsson et al., 2005), and also showed a general increase with RH but with a shoulder around RH = 50% where  
327 the observed  $\gamma(\text{HO}_2)$  also contained a small dip.

328 Values of  $\gamma(\text{N}_2\text{O}_5)$  (Tang et al., 2014) and  $\gamma(\text{ClONO}_2)$  (Tang et al., 2016) onto  $\text{TiO}_2$  particles were an order of  
329 magnitude lower than  $\gamma(\text{HO}_2)$  and may be associated with the lower polarity of these molecules compared to  $\text{HO}_2$ . It  
330 is likely that, as with uptake of  $\text{HO}_2$ , both  $\text{N}_2\text{O}_5$  and  $\text{ClONO}_2$  react with  $\text{TiO}_2$  via complexing with bridging OH  
331 groups and adsorbed  $\text{H}_2\text{O}$ , therefore less polar molecules will be less bound to the surface and more likely to desorb  
332 back into the gas phase, leading to a smaller  $\gamma$ . The dependence of  $\gamma(\text{N}_2\text{O}_5)$  for  $\text{TiO}_2$  with RH is also different to that  
333 for  $\text{HO}_2$  observed here, with a small decrease of  $\gamma(\text{N}_2\text{O}_5)$  observed as the RH is increased from  $\sim 5 - 23\%$  where a  
334 minimum is reached, then beyond 23%  $\gamma(\text{N}_2\text{O}_5)$  increases as RH is increased. (Tang et al., 2014). Competition  
335 between water and  $\text{N}_2\text{O}_5$  for surface active OH groups was suggested for the initial observed decrease in  $\gamma(\text{N}_2\text{O}_5)$   
336 with RH, whereas for RH  $> \sim 23\%$  heterogeneous hydrolysis of  $\text{N}_2\text{O}_5$  to form  $\text{HNO}_3$  starts to drive reactive uptake  
337 resulting in an increase of  $\gamma(\text{N}_2\text{O}_5)$  (Tang et al., 2014). Measurements of  $\gamma(\text{ClONO}_2)$  onto  $\text{TiO}_2$  particles were only  
338 made at two values of RH, insufficient to determine any systematic dependence, although Tang *et al.* (2016) expected  
339  $\gamma(\text{ClONO}_2)$  to increase as more water adsorbs onto the surface of  $\text{TiO}_2$  particles.

340 Measurements of  $\gamma(\text{HO}_2)$  have been made onto sulphuric acid aerosols and thin films. These values are not consistent  
341 and range from  $> 0.1$  to  $< 0.01$  (Cooper and Abbatt, 1996; Thornton and Abbatt, 2005; Hanson et al., 1992; Gershenson  
342 et al., 1995). The most recent measurement of  $\gamma(\text{HO}_2)$  on aqueous phase sulphuric acid aerosols was conducted at  
343 35% RH (Thornton and Abbatt, 2005). That study estimated a value of  $\gamma(\text{HO}_2) = 0.006 \pm 0.004$ , lower than onto  
344  $\text{TiO}_2$  aerosols. Whilst the aerosols in that study are unlike sulphuric acid aerosols in the stratosphere, formed via  
345 condensation of sulphuric acid vapour onto existing solid aerosols, the relatively low value of  $\gamma(\text{HO}_2)$  measured is

346 consistent with the likely low partitioning of HO<sub>2</sub> to its more reactive conjugate base, O<sub>2</sub><sup>-</sup>, and a lower solubility of  
347 HO<sub>2</sub> in aerosols with a low pH. The study concludes that heterogeneous uptake of HO<sub>2</sub> onto sulphuric acid aerosols  
348 would show a strong negative temperature dependence driven by the temperature dependence of the Henry's Law  
349 coefficient. It is likely that at temperatures typical of the lower stratosphere (205 – 215 K)  $\gamma(\text{HO}_2)$  onto sulphuric  
350 acid particles approach 1 (Gershenson et al., 1995).

351 George et al. (2013) previously measured  $\gamma(\text{HO}_2)$  onto dry salt aerosols. Values of  $\gamma(\text{HO}_2)$  for NaCl and (NH<sub>4</sub>)<sub>2</sub>SO<sub>4</sub>  
352 at RH values (33 – 54%) below their deliquescence point were below the limit of detection ( $\gamma(\text{HO}_2) < 0.004$ ). Values  
353 of  $\gamma(\text{HO}_2)$  for TiO<sub>2</sub> reported here (Figure 4 and Table 1) are more than an order of magnitude greater than that of  
354 solid salts, even for RH = 11%. A possible explanation for the difference in  $\gamma(\text{HO}_2)$  values could be that even though  
355 the sizes of the aerosols determined by the SMPS are similar, dry salt aerosols are more spherical in shape than TiO<sub>2</sub>  
356 particles which may be more fractal in nature. As the SMPS indirectly measures the surface area of aerosols by  
357 measuring their mobility through an electric field, an assumption that the aerosol is spherical has to be made. If this  
358 is not the case, this may lead to a significant under-prediction of the surface area of non-spherical aerosols and  
359 therefore an over-prediction of  $\gamma(\text{HO}_2)$ . In order to measure the geometry of the TiO<sub>2</sub> particles, a scanning electron  
360 microscope (SEM, FEI Nova NanoSEM 450) operating at 3 kV was used to image the TiO<sub>2</sub> nanoparticles used within  
361 these experiments. Samples for the SEM were prepared by dispersing the nanoparticles in ethanol and allowing a  
362 drop of this solution to dry on a silicon wafer. The wafer with nanoparticles was then mounted on SEM stubs using  
363 conductive carbon tapes and coated with 2 nm of Ir, using a Cressington 208HR high resolution sputter coater. Figure  
364 7 shows an example of an SEM image providing evidence that the TiO<sub>2</sub> particles are spherical and therefore any error  
365 associated with SMPS measurements of surface area is minimal. A more likely explanation for the higher  $\gamma(\text{HO}_2)$   
366 for TiO<sub>2</sub> particles is that dry salt aerosols do not adsorb a significant amount of water onto their surface until the  
367 deliquescence point reached, whereas at RH = 11% Figure 4 shows that the TiO<sub>2</sub> particles already have a monolayer  
368 coverage which can form relatively strongly bound complexes with HO<sub>2</sub>. Measurements of  $\gamma(\text{HO}_2)$  onto aqueous salt  
369 aerosols show that  $\gamma(\text{HO}_2)$  significantly increases above the deliquescence point (George et al., 2013) and is  
370 comparable to  $\gamma(\text{HO}_2)$  measured for TiO<sub>2</sub> ( $\gamma(\text{HO}_2) \sim 0.01$ ).



371

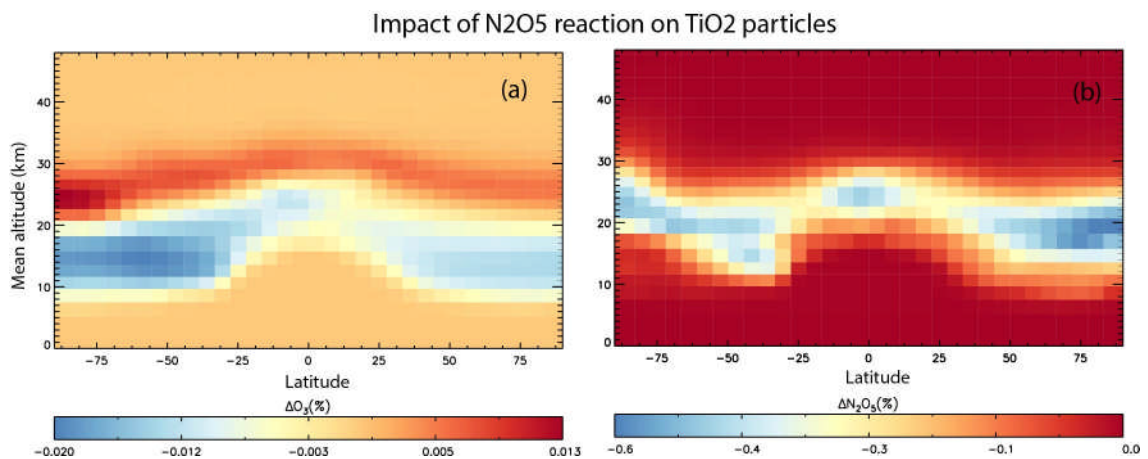
372 **Figure7.** SEM image of a single TiO<sub>2</sub> particle magnified 80,000× used within this study.

### 373 **3.3 Implications of HO<sub>2</sub> uptake by TiO<sub>2</sub> for stratospheric chemistry**

374 The effect of HO<sub>2</sub> uptake onto TiO<sub>2</sub> particles upon the stratospheric concentrations of HO<sub>2</sub> and O<sub>3</sub> was assessed using  
375 the TOMCAT model (Chipperfield, 1999, 2006). At RH relevant to the lower stratosphere (< 40%) the measurements  
376 showed that  $\gamma(\text{HO}_2)$  is in the range 0.020 - 0.028 at 295 K. An inverse temperature dependence of  $\gamma(\text{HO}_2)$  onto dry  
377 sea-salt aerosols has previously been observed (Remorov et al., 2002), and although there have been no systematic  
378 experimental studies of the temperature dependence of  $\gamma(\text{HO}_2)$ , parameterisations have developed (Thornton et al.,  
379 2008;Macintyre and Evans, 2011). At stratospherically relevant temperatures ( $T = 200 - 220$  K),  $\gamma(\text{HO}_2)$  is likely to  
380 be considerably larger than observed at 295 K, however it is not possible to cool the aerosol flow tube/SMPS system  
381 to verify this experimentally. Therefore  $\gamma(\text{HO}_2) = 1$  was used in the model simulations representing an upper limit,  
382 with three TOMCAT simulations performed as follows. A control simulation, similar to that presented in  
383 Chipperfield et al. (2015) did not include TiO<sub>2</sub> particles. A specified latitude-height distribution of TiO<sub>2</sub> particles was  
384 then included in two simulations with an effective aerosol surface area density equal to that of sulphate aerosols in  
385 1992 the year after the eruption of Mt. Pinatubo. This is an assumption which allows for the fact that less TiO<sub>2</sub> mass  
386 is needed in order to produce the same radiative impact as sulphate aerosol from Mt. Pinatubo, but the TiO<sub>2</sub> particle  
387 size is smaller. Hence these effects largely cancel (Tang et al., 2014). Stratospheric injection via a geo-engineering  
388 solution will result initially in a different distribution of TiO<sub>2</sub> particles compared with after the Mt. Pinatubo eruption,  
389 but it is assumed that following mixing and transport the distributions would resemble one another and not lead to  
390 any significant difference in model behaviour and the conclusions drawn. Support from this assumption comes from  
391 a model run in which a globally uniform distribution of TiO<sub>2</sub> was assumed initially and which yielded very similar  
392 results.

393 The first of these simulations included only the loss of N<sub>2</sub>O<sub>5</sub> on TiO<sub>2</sub> particles with  $\gamma(\text{N}_2\text{O}_5) = 0.005$ , the upper limit  
394 used in the modelling of Tang et al. (2014), which allows us to compare our results with their study. The second TiO<sub>2</sub>  
395 simulation also included the loss of HO<sub>2</sub> on TiO<sub>2</sub> particles with a  $\gamma(\text{HO}_2) = 1$ , as discussed above. Figure 8 shows  
396 the impact of including heterogeneous loss of N<sub>2</sub>O<sub>5</sub> on TiO<sub>2</sub> particles in the model.

397



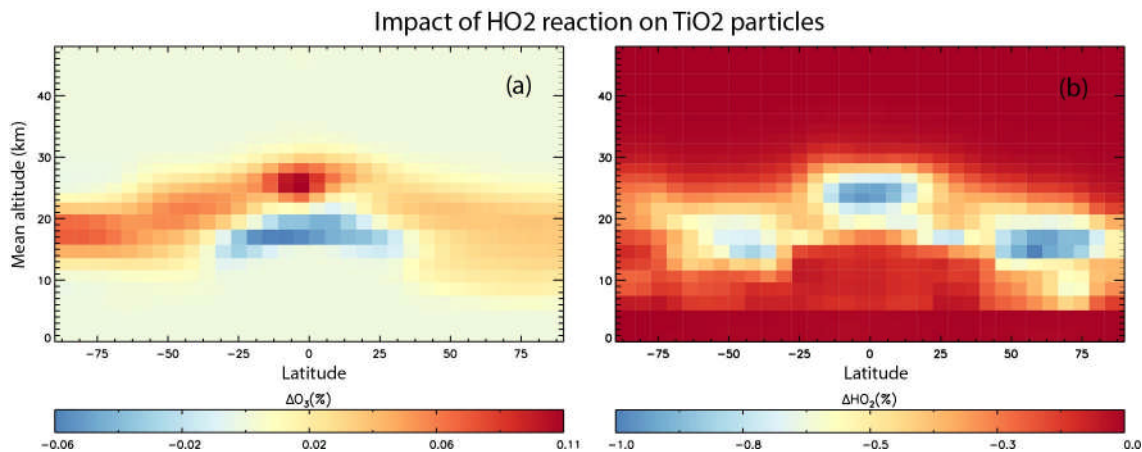
399 **Figure 8.** Annual mean change (%) in atmospheric O<sub>3</sub> (a) and N<sub>2</sub>O<sub>5</sub> (b) calculated using the TOMCAT 3-D model  
400 from inclusion of heterogeneous loss of N<sub>2</sub>O<sub>5</sub> on TiO<sub>2</sub> particles for 2008 and using  $\gamma(\text{N}_2\text{O}_5) = 0.005$ .

401

402 N<sub>2</sub>O<sub>5</sub> is decreased by up to 0.5% in the region of TiO<sub>2</sub> particles, which is assumed to follow the distribution of  
403 sulphate particles after the Mt. Pinatubo eruption, in order to follow the approach of previous modelling studies.  
404 Assuming a globally uniform distribution initially yielded results that were very similar. Inclusion of uptake is only  
405 a minor effect and considerably smaller than the impact of around -20% modelled by Tang et al. (2004) for the same  
406 assumed  $\gamma(\text{N}_2\text{O}_5) = 0.005$ . The reasons for this are not clear, although it is noted that the effect modelled in our off-  
407 line chemical transport model, with specified meteorology, is clearly confined to regions of high aerosol loading.  
408 The impacts modelled in the nudged chemistry-climate model study of Tang et al. (2004) are not confined to the  
409 region of high aerosol and even extend to the upper stratosphere. It is possible that their simulations, although nudged,  
410 also include some dynamical feedback which enhances an otherwise small signal. Figure 8 also shows that the  
411 resulting impact on O<sub>3</sub> is small with changes less than 0.02%. The model produces a region of slight decrease in the  
412 very low stratosphere, with a region of slight increase above.

413 Figure 9 shows results from the simulation which also included the loss of HO<sub>2</sub> on stratospheric TiO<sub>2</sub> particles, and  
414 using  $\gamma(\text{HO}_2) = 1$  (a simulation using the measured value of  $\gamma(\text{HO}_2) = 0.021$  at 295 K led to no impact on O<sub>3</sub> or HO<sub>2</sub>).

415



416

417 **Figure 9.** Annual mean change (%) in atmospheric O<sub>3</sub> (a) and HO<sub>2</sub> (b) calculated using the TOMCAT 3-D model  
418 from inclusion of heterogeneous loss of HO<sub>2</sub> on TiO<sub>2</sub> particles for 2008, and using  $\gamma(\text{HO}_2) = 1$ .

419

420 It is evident that HO<sub>2</sub> loss due to heterogeneous reaction between HO<sub>2</sub> and TiO<sub>2</sub> particles in 2008 is < 1% and is  
421 confined to the lower stratosphere where it is assumed TiO<sub>2</sub> particles are located. Figure 9 also shows that the  
422 subsequent effect of the TiO<sub>2</sub> particles on the O<sub>3</sub> concentrations through the effects of this reaction is also small  
423 (< 0.1%), with a small decrease in the tropical upper troposphere/lower stratosphere and a small increase at all



424 latitudes in the lower stratosphere. This small effect of TiO<sub>2</sub> particles on stratospheric HO<sub>2</sub> and O<sub>3</sub> concentrations is  
425 due to the reactive nature and short lifetime of HO<sub>2</sub>. The species readily reacts with other gas phase species (e.g. O<sub>3</sub>)  
426 and so loss on TiO<sub>2</sub> surfaces does not compete significantly.

427

#### 428 **4. Conclusions and further work**

429 The reactive uptake coefficients for the heterogeneous reaction of HO<sub>2</sub> onto TiO<sub>2</sub> particles were measured at different  
430 RH and at room temperature for the first time using an aerosol flow tube reactor coupled with a sensitive FAGE HO<sub>2</sub>  
431 detection system. A range of HO<sub>2</sub> uptake coefficients on TiO<sub>2</sub> particles were measured varying from  $\gamma(\text{HO}_2) = 0.021$   
432  $\pm 0.001$  to  $0.036 \pm 0.007$  for RH over the range 11% to 66%, respectively. The HO<sub>2</sub> uptake coefficient showed a  
433 positive dependence on RH which correlated well with the number of monolayers of water adsorbed onto the TiO<sub>2</sub>  
434 particle. These results suggest a mechanism by which HO<sub>2</sub> adsorbs to the surface of the TiO<sub>2</sub> particle by forming  
435 complexes with water molecules bound to bridging OH groups. As the number of water layers increases so does the  
436 network of hydrogen bonds that stabilises HO<sub>2</sub> leading to a longer adsorption lifetime and increased  $\gamma(\text{HO}_2)$ . The  
437 TOMCAT chemical transport model was used to evaluate the possible effects of HO<sub>2</sub> uptake (using an upper limit of  
438  $\gamma(\text{HO}_2) = 1$ ) onto the surface of TiO<sub>2</sub> particles on the stratospheric concentrations of HO<sub>2</sub> and O<sub>3</sub>. The amount of  
439 TiO<sub>2</sub> used was chosen to achieve a similar cooling to that following the Mt. Pinatubo eruption, but the model predicted  
440 a very small loss of both stratospheric HO<sub>2</sub> and O<sub>3</sub>. TiO<sub>2</sub> possesses photocatalytic properties and water adsorbed  
441 onto its surface may dissociate under stratospheric illumination providing a source of radicals (Chen et al.,  
442 2012; Romanias et al., 2012). Production of OH and HO<sub>2</sub> from irradiated TiO<sub>2</sub> surfaces should be evaluated in future  
443 studies together with studies of uptake at lower temperature to fully understand the consequences of injection of TiO<sub>2</sub>  
444 particles into the stratosphere.

445

#### 446 **Acknowledgements**

447 We are grateful to the Natural Environment Research Council for funding a studentship (DRM) and for funding the  
448 aerosol flow tube apparatus (grant number NE/F020651/1). LKW, TI, PWS and DEH are also grateful to the  
449 NERC funded National Centre for Atmospheric Science for ongoing support. The TOMCAT modelling work was  
450 supported by the EU StratoClim project (FP7 grant 603557). We thank Wuhu Feng (NCAS Leeds) for help with the  
451 model. The model simulations were performed on the University of Leeds and N8 HPC system.

452

453 **References**

- 454 Aloisio, S., and Francisco, J. S.: Existence of a hydroperoxy and water ( $\text{HO}_2$  center dot  $\text{H}_2\text{O}$ ) radical complex,  
455 *Journal of Physical Chemistry A*, 102, 1899-1902, 10.1021/jp972173p, 1998.
- 456 Ammann, M., Cox, R. A., Crowley, J. N., Jenkin, M. E., Mellouki, A., Rossi, M. J., Troe, J., and Wallington, T. J.:  
457 Evaluated kinetic and photochemical data for atmospheric chemistry: Volume VI - heterogeneous reactions with  
458 liquid substrates, *Atmos Chem Phys*, 13, 8045-8228, 10.5194/acp-13-8045-2013, 2013.
- 459 Anpo, M., Che, M., Fubini, B., Garrone, E., Giamello, E., and Paganini, M. C.: Generation of superoxide ions at  
460 oxide surfaces, *Topics in Catalysis*, 8, 189, 10.1023/a:1019117328935, 1999.
- 461 Bedjanian, Y., Romanias, M. N., and El Zein, A.: Uptake of  $\text{HO}_2$  radicals on Arizona Test Dust, *Atmos Chem*  
462 *Phys*, 13, 6461-6471, 10.5194/acp-13-6461-2013, 2013.
- 463 Brown, R. L.: Tubular flow reactors with 1st-order kinetics, *Journal of Research of the National Bureau of*  
464 *Standards*, 83, 1-8, 1978.
- 465 Chen, H., Nanayakkara, C. E., and Grassian, V. H.: Titanium Dioxide Photocatalysis in Atmospheric Chemistry,  
466 *Chem. Rev.*, 112, 5919-5948, 10.1021/cr3002092, 2012.
- 467 Chipperfield, M. P.: Multiannual simulations with a three-dimensional chemical transport model, *J. Geophys. Res.-*  
468 *Atmos.*, 104, 1781-1805, 10.1029/98jd02597, 1999.
- 469 Chipperfield, M. P.: New version of the TOMCAT/SLIMCAT off-line chemical transport model: Intercomparison  
470 of stratospheric tracer experiments, *Q. J. R. Meteorol. Soc.*, 132, 1179-1203, 10.1256/qj.05.51, 2006.
- 471 Chipperfield, M. P., Dhomse, S. S., Feng, W., McKenzie, R. L., Velders, G. J. M., and Pyle, J. A.: Quantifying the  
472 ozone and ultraviolet benefits already achieved by the Montreal Protocol, *Nat. Commun.*, 6, 8,  
473 10.1038/ncomms8233, 2015.
- 474 Cooper, P. L., and Abbatt, J. P. D.: Heterogeneous interactions of OH and  $\text{HO}_2$  radicals with surfaces characteristic  
475 of atmospheric particulate matter, *Journal of Physical Chemistry*, 100, 2249-2254, 1996.
- 476 Dutton, E. G., and Christy, J. R.: Solar radiative forcing at selected locations and evidence for global lower  
477 tropospheric cooling following the eruptions of El-Chichon and Pinatubo, *Geophysical Research Letters*, 19, 2313-  
478 2316, 10.1029/92gl02495, 1992.
- 479 Fuchs, N. A., and Sutugin, A. G.: Highly dispersed aerosols, Ann Arbor Science, London, 1970.
- 480 George, I. J., Matthews, P. S., Whalley, L. K., Brooks, B., Goddard, A., Baeza-Romero, M. T., and Heard, D. E.:  
481 Measurements of uptake coefficients for heterogeneous loss of  $\text{HO}_2$  onto submicron inorganic salt aerosols, *Phys*  
482 *Chem Chem Phys*, 15, 12829-12845, 10.1039/c3cp51831k, 2013.
- 483 Gershenzon, Y. M., Grigorieva, V. M., Ivanov, A. V., and Remorov, R. G.:  $\text{O}_3$  and OH sensitivity to heterogeneous  
484 sinks of  $\text{HO}_x$  and  $\text{CH}_3\text{O}_2$  on aerosol particles, *Faraday Discussions*, 100, 83-100, 1995.
- 485 Goodman, A. L., Bernard, E. T., and Grassian, V. H.: Spectroscopic study of nitric acid and water adsorption on  
486 oxide particles: Enhanced nitric acid uptake kinetics in the presence of adsorbed water, *Journal of Physical*  
487 *Chemistry A*, 105, 6443-6457, 10.1021/jp0037221, 2001.
- 488 Gustafsson, R. J., Orlov, A., Badger, C. L., Griffiths, P. T., Cox, R. A., and Lambert, R. M.: A comprehensive  
489 evaluation of water uptake on atmospherically relevant mineral surfaces: DRIFT spectroscopy, thermogravimetric  
490 analysis and aerosol growth measurements, *Atmos Chem Phys*, 5, 3415-3421, 2005.
- 491 Hanson, D. R., Burkholder, J. B., Howard, C. J., and Ravishankara, A. R.: Measurement of hydroxyl and  
492 hydroperoxy radical uptake coefficients on water and sulfuric acid surfaces, *The Journal of Physical Chemistry*, 96,  
493 4979-4985, 10.1021/j100191a046, 1992.
- 494 Heard, D. E., and Pilling, M. J.: Measurement of OH and  $\text{HO}_2$  in the troposphere, *Chem. Rev.*, 103, 5163-5198,  
495 2003.
- 496 Holloway, A. M., and Wayne, R. P.: *Atmospheric Chemistry*, Royal Society of Chemistry, 2010.
- 497 Huneus, N., Schulz, M., Balkanski, Y., Griesfeller, J., Prospero, J., Kinne, S., Bauer, S., Boucher, O., Chin, M.,  
498 Dentener, F., Diehl, T., Easter, R., Fillmore, D., Ghan, S., Ginoux, P., Grini, A., Horowitz, L., Koch, D., Krol, M.  
499 C., Landing, W., Liu, X., Mahowald, N., Miller, R., Morcrette, J. J., Myhre, G., Penner, J., Perlwitz, J., Stier, P.,  
500 Takemura, T., and Zender, C. S.: Global dust model intercomparison in AeroCom phase I, *Atmos Chem Phys*, 11,  
501 7781-7816, 10.5194/acp-11-7781-2011, 2011.
- 502 Joshi, R., and Ghanty, T. K.: Hydrogen bonding interaction between  $\text{HO}_2$  radical and selected organic acids,  
503  $\text{RCOOH}$  ( $\text{R} = \text{CH}_3, \text{H}, \text{Cl}$  and  $\text{F}$ ), *Chem. Phys. Lett.*, 584, 43-48, 10.1016/j.cplett.2013.08.025, 2013.
- 504 Karagulian, F., Santschi, C., and Rossi, M. J.: The heterogeneous chemical kinetics of  $\text{N}_2\text{O}_5$  on  $\text{CaCO}_3$  and other  
505 atmospheric mineral dust surrogates, *Atmos Chem Phys*, 6, 1373-1388, 2006.
- 506 Ketteler, G., Yamamoto, S., Bluhm, H., Andersson, K., Starr, D. E., Ogletree, D. F., Ogasawara, H., Nilsson, A.,  
507 and Salmeron, M.: The nature of water nucleation sites on  $\text{TiO}_2(110)$  surfaces revealed by ambient pressure X-ray  
508 photoelectron spectroscopy, *J. Phys. Chem. C*, 111, 8278-8282, 10.1021/jp068606i, 2007.

509 Lakey, P. S. J., George, I. J., Baeza-Romero, M. T., Whalley, L. K., and Heard, D. E.: Organics Substantially  
510 Reduce HO<sub>2</sub> Uptake onto Aerosols Containing Transition Metal ions, *Journal of Physical Chemistry A*, 120, 1421-  
511 1430, 10.1021/acs.jpca.5b06316, 2016.

512 Macintyre, H. L., and Evans, M. J.: Parameterisation and impact of aerosol uptake of HO<sub>2</sub> on a global tropospheric  
513 model, *Atmos Chem Phys*, 11, 10965-10974, 10.5194/acp-11-10965-2011, 2011.

514 Matthews, P. S. J., Baeza-Romero, M. T., Whalley, L. K., and Heard, D. E.: Uptake of HO<sub>2</sub> radicals onto Arizona  
515 test dust particles using an aerosol flow tube, *Atmos Chem Phys*, 14, 7397-7408, 10.5194/acp-14-7397-2014, 2014.

516 McCormick, M. P., Thomason, L. W., and Trepte, C. R.: Atmospheric effects of the Mt. Pinatubo eruption, *Nature*,  
517 373, 399-404, 10.1038/373399a0, 1995.

518 Pope, F. D., Braesicke, P., Grainger, R. G., Kalberer, M., Watson, I. M., Davidson, P. J., and Cox, R. A.:  
519 Stratospheric aerosol particles and solar-radiation management, *Nat. Clim. Chang.*, 2, 713-719,  
520 10.1038/nclimate1528, 2012.

521 Remorov, R. G., Gershenzon, Y. M., Molina, L. T., and Molina, M. J.: Kinetics and mechanism of HO<sub>2</sub> uptake on  
522 solid NaCl, *Journal of Physical Chemistry A*, 106, 4558-4565, 10.1021/jp013179o, 2002.

523 Romanias, M. N., El Zein, A., and Bedjanian, Y.: Heterogeneous Interaction of H<sub>2</sub>O<sub>2</sub> with TiO<sub>2</sub> Surface under Dark  
524 and UV Light Irradiation Conditions, *Journal of Physical Chemistry A*, 116, 8191-8200, 10.1021/jp305366v, 2012.

525 Shepherd, J. G., and Working Group on Geoengineering the Climate: Geoengineering the climate: science,  
526 governance and uncertainty, Project Report, 2009.

527 Tang, M., Keeble, J., Telford, P. J., Pope, F. D., Braesicke, P., Griffiths, P. T., Abraham, N. L., McGregor, J.,  
528 Watson, I. M., Cox, R. A., Pyle, J. A., and Kalberer, M.: Heterogeneous reaction of ClONO<sub>2</sub> with TiO<sub>2</sub> and SiO<sub>2</sub>  
529 aerosol particles: implications for stratospheric particle injection for climate engineering, *Atmos. Chem. Phys.*, 16,  
530 15397-15412, 10.5194/acp-16-15397-2016, 2016.

531 Tang, M. J., Telford, P. J., Pope, F. D., Rkiouak, L., Abraham, N. L., Archibald, A. T., Braesicke, P., Pyle, J. A.,  
532 McGregor, J., Watson, I. M., Cox, R. A., and Kalberer, M.: Heterogeneous reaction of N<sub>2</sub>O<sub>5</sub> with airborne TiO<sub>2</sub>  
533 particles and its implication for stratospheric particle injection (vol 14, pg 6035, 2014), *Atmos Chem Phys*, 14,  
534 8233-8234, 10.5194/acp-14-8233-2014, 2014.

535 Textor, C., Schulz, M., Guibert, S., Kinne, S., Balkanski, Y., Bauer, S., Berntsen, T., Berglen, T., Boucher, O.,  
536 Chin, M., Dentener, F., Diehl, T., Easter, R., Feichter, H., Fillmore, D., Ghan, S., Ginoux, P., Gong, S.,  
537 Kristjansson, J. E., Krol, M., Lauer, A., Lamarque, J. F., Liu, X., Montanaro, V., Myhre, G., Penner, J., Pitari, G.,  
538 Reddy, S., Seland, O., Stier, P., Takemura, T., and Tie, X.: Analysis and quantification of the diversities of aerosol  
539 life cycles within AeroCom, *Atmos Chem Phys*, 6, 1777-1813, 2006.

540 Thornton, J., and Abbatt, J. P. D.: Measurements of HO<sub>2</sub> uptake to aqueous aerosol: Mass accommodation  
541 coefficients and net reactive loss, *J. Geophys. Res.-Atmos.*, 110, 10.1029/2004jd005402, 2005.

542 Thornton, J. A., Jaegle, L., and McNeill, V. F.: Assessing known pathways for HO<sub>2</sub> loss in aqueous atmospheric  
543 aerosols: Regional and global impacts on tropospheric oxidants, *J. Geophys. Res.-Atmos.*, 113,  
544 10.1029/2007jd009236, 2008.

545 Usher, C. R., Michel, A. E., Stec, D., and Grassian, V. H.: Laboratory studies of ozone uptake on processed mineral  
546 dust, *Atmos. Environ.*, 37, 5337-5347, 10.1016/j.atmosenv.2003.09.014, 2003.

547 Versick, S., Stiller, G. P., von Clarmann, T., Reddmann, T., Glatthor, N., Grabowski, U., Hoepfner, M., Kellmann,  
548 S., Kiefer, M., Linden, A., Ruhnke, R., and Fischer, H.: Global stratospheric hydrogen peroxide distribution from  
549 MIPAS-Envisat full resolution spectra compared to KASIMA model results, *Atmos Chem Phys*, 12, 4923-4933,  
550 10.5194/acp-12-4923-2012, 2012.

551 Visioni, D., Pitari, G., and Aquila, V.: Sulfate geoengineering: a review of the factors controlling the needed  
552 injection of sulfur dioxide, *Atmos. Chem. Phys.*, 17, 3879-3889, 10.5194/acp-17-3879-2017, 2017.

553 Wennberg, P. O., Cohen, R. C., Stimpfle, R. M., Koplw, J. P., Anderson, J. G., Salawitch, R. J., Fahey, D. W.,  
554 Woodbridge, E. L., Keim, E. R., Gao, R. S., Webster, C. R., May, R. D., Toohey, D. W., Avallone, L. M., Proffitt,  
555 M. H., Loewenstein, M., Podolske, J. R., Chan, K. R., Wofsy, S. C.: Removal of stratospheric O<sub>3</sub> by radicals - in  
556 situ measurements of OH, HO<sub>2</sub>, NO, NO<sub>2</sub>, ClO, and BrO, *Science*, 266, 398-404, 10.1126/science.266.5184.398,  
557 1994.

558 Winiberg, F. A. F., Smith, S. C., Bejan, I., Brumby, C. A., Ingham, T., Malkin, T. L., Orr, S. C., Heard, D. E., and  
559 Seakins, P. W.: Pressure-dependent calibration of the OH and HO<sub>2</sub> channels of a FAGE HO<sub>x</sub> instrument using the  
560 Highly Instrumented Reactor for Atmospheric Chemistry (HIRAC), *Atmos. Meas. Tech.*, 8, 523-540, 10.5194/amt-  
561 8-523-2015, 2015.

562 Yamamoto, S., Bluhm, H., Andersson, K., Ketteler, G., Ogasawara, H., Salmeron, M., and Nilsson, A.: In situ x-  
563 ray photoelectron spectroscopy studies of water on metals and oxides at ambient conditions, *J. Phys.-Condes.*  
564 Matter, 20, 14, 10.1088/0953-8984/20/18/184025, 2008.

